Scaling Relations of Star-forming Galaxies since $z \sim 1$

Gauri Sharma,[1, 2, 3, ★] and Paolo Salucci[1, 2, 3]

[1] SISSA International School for Advanced Studies, Via Bonomea 265, I-34136 Trieste, Italy
[2] GSKY, INFN-Sezione di Trieste, via Valerio 2, I-34127 Trieste, Italy
[3] IFPU Institute for Fundamental Physics of the Universe, Via Beirut, 2, 34151 Trieste, Italy

ABSTRACT

Context. Studying the scaling relationships of galaxies across cosmic timescales is crucial to understanding the formation and evolution of galaxies. Recent observational studies show that as we go further back in time ($z > 0.5$), rotation-supported star-forming galaxies (SFGs) exhibit a turbulent interstellar medium in which pressure dominates, which supports the stellar disc against gravity such that the disc begins to rotate slowly. Under such peculiar conditions, what happens to the seminal scaling relations?
Aims. We studied the behaviour of seminal scaling relation at $z \sim 1$ star-forming galaxies. Especially, stellar Tully-Fisher relation, mas-size, and specific angular momentum relation.
Methods. We investigate a sub-sample of KMOS Redshift One Spectroscopic Survey (KROSS), which has been studied by Sharma et al. (2021a). We studied 250 rotation supported star-forming disc-like galaxies at $z \approx 0.9$ having stellar mass range: $9.0 \leq log(M_* \, \mathrm{M_\odot}) \leq 11.0$ and star formation rate: $0.49 \leq log\left(SFR\,[\mathrm{M_\odot \, yr^{-1}}]\right) \leq 1.77$. The stellar masses ($M_*$) of these objects are obtained previously using mass-to-light ratio derived from spectral energy distribution fitting of the galaxies. The star-formation rates are derived from $\mathrm{H_\alpha}$ luminosities. The circular velocities are obtained directly from the rotation curves at $2.95R_e$.
Results. We find that $z \sim 1$ star-forming disc-like systems exhibit the same mass-size relations as locals disc galaxies, as well as a similar scaling of the specific stellar angular momentum with stellar mass. This confirms the results of previous studies suggesting that the baryon assembly functions in a similar way at all epochs ($0 < z < 3$). On the other hand, we noticed a significant evolution in the slope of the stellar Tully-Fisher relation at $z \sim 1$, while its zero-point remains the same as for local disc galaxies.
Conclusions. We report a divergent evolution of the stellar Tully-Fisher relation, suggesting that (1) the interaction (gravitational or collisional) of baryons and dark matter is an environment- and time-dependent process. (2) with respect to local disc galaxies, the dark matter halos at $z \sim 1$ are denser within the stellar disc.

Key words. galaxies: kinematics and dynamics;– galaxies: late-type, disk-type and rotation dominated; – galaxies: evolution; – galaxies: dark matter halo;– cosmology: nature of dark matter

1. Introduction

Although galactic processes are complex and show diversity from one galaxy type to another, there are some fundamental properties (in terms of kinematics and dynamics) that correlate over a large range (several orders of magnitude) of a galaxy type (late and early types). The correlation between the fundamental properties (mass, velocity, and scale-radius) of galaxies, often referred to as *scaling relations*, and are thought to play an important role in galaxy evolution. Indeed, they are the benchmark for current theoretical predictions (and semi-analytical modelling) of galaxy formation and evolution. Therefore, the study of scaling relations and their cosmic evolution is an intriguing subject for both astrophysicists and cosmologists, and one which always remains disputable. In this work, I have continued the long tradition of studying scaling relations, in particular, I have studied Tully-Fisher relation of disc galaxies and shown it's cosmic evolution since $z \sim 1$.

The Tully-Fisher Relation (TFR) is the most fundamental empirical scaling relation which correlates the luminous matter properties with the dark halo. In the traditional TFR, which came from the seminal work of Tully & Fisher (in 1977), luminosity of the galaxies scales with their characteristic velocity (i.e. circular velocity V_c) via power-law $L \propto \beta V_c^\alpha$, where α is the slope, and β

is intercept in the relation. Here, slope tells us the extent of circular velocity dependency on the luminosity, while quantity (β/α) is the zero-point which tells us the origin of this relation. In the local universe, this relation is remarkably tight ($\alpha \sim 4; \beta/\alpha \sim 2$) for star-forming disc galaxies (Tully & Fisher 1977; Feast 1994; Bell & de Jong 2001; Karachentsev et al. 2002; Pizagno et al. 2007; Toribio et al. 2011; McGaugh et al. 2000; Sorce et al. 2013). Therefore, it is widely used in the redshift independent distance measurements (Giovanelli et al. 1997b; Ferrarese et al. 2000; Freedman et al. 2011; Sorce et al. 2013; Neill et al. 2014). Since by knowing the luminosity one can relate the observed flux via $L \propto F/4\pi D^2$ and infer the distance of the object. Moreover, TFR has also played an important role in determining the cosmological parameters, in particular by allowing the measurement of the Hubble constant H_0 out to the local Universe (Giovanelli et al. 1997a; Tully & Pierce 2000; Masters et al. 2006).

Beyond the distance indicator and cosmological needs, TFR is also widely discussed to understand the Galaxy formation and Evolution theory. In fact, it is one of the first scaling relations which explains the interplay of dark and luminous matter in the local Universe with a wide variety of data (Mathewson et al. 1992; McGaugh et al. 2000; McGaugh 2005; Papastergis et al. 2016; Lapi et al. 2018) and simulations (Mo & Mao 2000; Steinmetz & Navarro 1999). The rationale here is that- the circular velocity is related to the total gravitational potential of the

★ Contact: gsharma@sissa.it

galaxy while luminosity traces the total stellar mass (Blumenthal et al. 1984; Mao et al. 1998; Girardi et al. 2002). This conception gives the birth to modified TFR: $M \propto \beta V_c^\alpha$ (where M is the stellar or baryonic mass of the galaxy) which is well studied and proven remarkably tight in the local Universe (Verheijen & Sancisi 2001; McGaugh 2005; de Blok et al. 2008; Stark et al. 2009; Foreman & Scott 2012; Lelli et al. 2016; Papastergis et al. 2016; Lapi et al. 2018; Lelli et al. 2019). With the words of caution, in the optical and infra-red astronomy luminosity traces the stellar mass, which leads to stellar-TFR (STFR). Whereas, luminosity in the radio-wavelength traces the gas mass which in combination with stellar mass gives us nearly total baryonic mass ($M_B = M_* + M_{gas}$) of the system and thus the relation is referred as baryonic-TFR (BTFR). Besides it, under the assumption that motion of baryons is circular in the Dark Matter (DM) halo, TFR also relates the total luminosity of galaxy via its total circular velocity, mass surface density (Σ), and mass-to-light ratio ($M/L = \Upsilon^*$) given by $L \propto V_c / (\Sigma \Upsilon^*)$ (Binney & Tremaine 2008). This relation gives us a simplistic way to infer the relative difference in mass-to-light ratio and surface-density of different sub-classes of galaxies. Therefore, TFR is not only useful as distance indicator but also put the stringent constraints on the galaxy formation and evolution models and DM properties. The position of a galaxy on L-V or M-V plane gives us a direct indication of "how efficiently gas converted into stars and what is total mass distribution in the galaxy". In short, TFR is the foundation of galaxy formation and evolution models; therefore, it should be capable of explaining baryons and dark matter interplay at any epoch, and if not, then we have to understand why?

In this work, we are exploring the TFR at $z \sim 1$ for star-forming galaxies (disk-like). Firstly, because a disk-type system form and evolve at $z \leq 1.5$ and shows the homogeneous and controlled evolution (e.g. Lagos et al. 2017), therefore, can be used as a cosmic ladder to infer the cosmic evolution of baryons and dark matter. Second, $z \sim 1$ is the epoch of transition where dark energy kicks-in and enforces the accelerated expansion of the Universe. It is known, nearly 50% of stellar mass in the Universe assembled in the galactic halos by $z \approx 1$ (Pérez-González et al. 2008), and this is the time where cosmic star-formation density peaks (Madau & Dickinson 2014, references therein). Therefore, it is crucial to compare the local baryonic and dark matter properties with the galaxies at $z \sim 1$. It will allow us to understand: (1) how the disk-type system evolves after their formation at $z \leq 1.5$, and (2) what is the nature of the dark matter in these systems concerning the local Universe?

Some of the previous studies of star-forming galaxies (hereafter SFGs) in the cluster environment Ziegler et al. (2002); Böhm et al. (2004), and van Starkenburg et al. (2006) have shown that the slope of TFR at intermediate redshift ($z \sim 0.5$) is shallower in comparison to locals and lead the discussion of selection bias effect. However, other studies have shown that there is nearly no evolution in TFR slope since $z \sim 1$ to $z \approx 0$ (Conselice et al. 2005; Kassin et al. 2007; Miller et al. 2011; Miller et al. 2012). Some recent studies of Integrated Field Unit (IFU) observations of isolated SFGs (Puech et al. 2008; Cresci et al. 2009; Gnerucci et al. 2011; Tiley et al. 2016; Übler et al. 2017; Harrison et al. 2017; Tiley et al. 2019b), claims that the zero-point of TFR varies while slope remains nearly the same. Therefore, currently, there is a chaos to reach on the conclusion of whether TFR has evolved over cosmic time (both in slope and zero-point) or it is just a selection effect. We would emphasize here that latter IFU studies have underlying uncertainties because: (1) Kinematics of datacubes has not been derived in 3D space. (2) There was a partial correction for beam smearing on the velocity profile. (3) They have not accounted for the pressure gradient corrections which dominates at high-z galaxies and suppress the circular velocity via radial-gradient. Notice, Übler et al. (2017) has accounted for the pressure gradient corrections but assuming constant and isotropic velocity dispersion, which overestimate the circular velocities (for details see Sharma et al. 2021a).

A quick recall, a telescope equipped with new generation spectrograph[1] can achieve only $0.5 - 1.0''$ spatial resolution, whereas, a galaxy from $z \sim 1$ has a typical angular size of $2'' - 3''$. Therefore, a finite beam size causes the line emission to smeared on the adjacent pixels. As a consequence, the gradient in the velocity fields tend to become flattened, and line emission began to broad, which creates a degeneracy in the calculation of rotation velocity and velocity dispersion. This effect in the observations is referred to as 'Beam Smearing', which affects the kinematic properties of the galaxies, i.e., underestimated rotation velocity and overestimated velocity dispersion. *On average, beam smearing correction increases the circular velocity by* $10 - 15\%$ (Johnson et al. 2018; Sharma et al. 2021a). On the other hand, at high-z Inter-Stellar Medium (ISM) is highly turbulent (Burkert et al. 2010; Wellons et al. 2020), this turbulence in the ISM induces a force against gravity in galactic disk via radial gradient which suppresses the rotation velocity of gas and stars. This effect generally referred to as 'Asymmetric Drift (AD)' for stellar component, and 'Pressure Gradient (PG)' for gas component. The latter effect is generally negligible in local rotation dominated galaxies (late-type galaxies) but significantly observed in the local dwarfs and early-type galaxies (e.g., Valenzuela et al. (2007); Read et al. (2016); Weijmans et al. (2008)). Highly turbulent ISM conditions and gas domination at high-z (Burkert et al. 2010; Turner et al. 2017; Johnson et al. 2018; Wellons et al. 2020) make pressure gradient prominent to disentangle, specifically, in the case of circular velocity measurements, dynamical mass modelling and DM studies. Otherwise, one may lead to underestimated circular velocity. *On average, AD or PG can suppress the rotation velocity by more than* 50% (see, Sharma et al. 2021a). Therefore, accurate Pressure Gradient Corrections (PGC) keeps more importance than the beam smearing correction.

Aforementioned physical and observational uncertainties have been disentangled by us in Sharma et al. (2021a). I this work, we adopt the kinematic and photometric dataset established in latter work. We also employ the dynamically estimated stellar and halo masses determined in Sharma et al. (2021c), thus improves upon the understanding of TFR at high-z. This paper organized as follows, section 2 contains a brief description of data and its physical quantities, section 3 describes the numerical recipe of fitting TFR and section 4 & 5 focused on the results and detailed discussion between current results and previous studies. The main findings of the work are summarized in section 6. In this work, we have assumed a flat ΛCDM cosmology with $\Omega_{m,0} = 0.27$, $\Omega_{\Lambda,0} = 0.73$ and $H_0 = 70 \; km \; s^{-1}$.

2. Data

We are using the KROSS star-forming galaxy sample previously studied by Stott et al. (2016) and others (Harrison et al. 2017; Tiley et al. 2019a,b; Johnson et al. 2018), this data is publicly available at KROSS-website[2]. From publicly available KROSS sample, a sub-sample of 344 star-forming galaxies is deeply in-

---

[1] Integrated Field Units (IFUs)
[2] http://astro.dur.ac.uk/KROSS/data.html

vestigated by Sharma et al. 2021a (hereafter, GS20). In GS20, kinematics of the KROSS datacubes is derived from ^{3D}BAROLO (Teodoro & Fraternali 2015; Di Teodoro et al. 2016). It takes into account the beam smearing correction in 3D-space and provides the moment maps, stellar surface brightness profile, rotation curve (RC), dispersion curve (DC) along with the kinematic models. Later RCs are corrected for pressure gradient, which seems to dominate the kinematics of high-z galaxies, for details we refer the reader to Sharma et al. (2021a). A two-step technique of handling datacubes in Sharma et al. (2021a) yields the intrinsic velocity profile of an individual galaxy even in the low-resolution data. Therefore gives us a robust and reliable estimate of the circular velocity of the sample. Out of 344 KROSS sample, we choose to analyse only 256 Quality-1 & 2 objects, referred to as Q12 sample in GS20 work.

In this work we adopt this Q12 sample, which we have also used to study the dark matter fraction in Sharma et al. (2021b). Let me remark, we adopt SED driven stellar masses (Tiley et al. 2019b), and total gas mass derived using Tacconi et al. (2018) and Lagos et al. (2011). Moreover, our sample is representative of *main-sequence* of star-forming galaxies. In Sharma et al. 2021c (under peer review), we further analyse the rotational curves (RCs) of Q12 and apply mass models to decompose the RCs into their constituents (stars gas and dark matter), thereby we study the structural properties of dark matter. In the latter work, we have also dynamically calculated the physical quantities (stellar mass & disc radius, virial mass & radius, and dark matter inner core density & radius) from individual and co-added RCs. Therefore, in this work, we use the photometric and kinematic data from Sharma et al. (2021a) and Sharma et al. (2021b), as well as the dynamically derived physical properties elaborated in Sharma et al. (2021c).

Since this work is partly focused on individual study of RCs; therefore, we visually inspect each RC and remove them if huge asymmetry is noticed. In total we discard six RCs. To resume, our final sample contains 250 galaxies, which covers the inclination range: $25° \le \theta_i \le 75°$, the redshift range: $0.75 \le z \le 1.04$, the effective radii: $0.12 \le \log(R_e \text{ [kpc]}) \le 1.04$, and circular velocities: $1.49 \le \log(V_{out} \text{ [km s}^{-1}]) \le 2.53$ computed at $R_{out}(\sim 3R_e)$. A distribution of circular velocities and stellar masses of Parent sample (Sharma et al. 2021a) and Q12 sample used in this work is shown in Figure[1]. As one can notice, we cover the full velocity ranges as used in Sharma et al. (2021a), so the KROSS parent Sample (Stott et al. 2016; Harrison et al. 2017).

3. Methodology and Analysis

In this section, we recall the circular velocities and stellar masses of the sample because they are the required quantities for Tully-Fisher relation. For the determination of other physical quantities, e.g. the radius of the stellar disk, we refer the reader to Harrison et al. (2017); Sharma et al. (2021a) and Sharma et al. (2021b). In addition, we also describe the fitting method used in constraining the Tully-Fisher relation slope and zero-point.

3.1. Velocity Measurements

We have investigated the circular velocity of rotation curves at four different scale lengths[3] R_e, R_{opt}, R_{out} (= 5 R_D) and R_{flat}[4] and referred to as V_c^{Re}, V_c^{opt}, V_c^{out} and V_c^{flat} respectively. Notice, effective radius for majority of sample falls below the resolution limit (~ 4.0 kpc with median seeing 0.5″ at $z \sim 0.9$), where as optical radius stays on the verge. To be conservative, we only rely on circular velocity measurements done at R_{out} and R_{flat}, those stays above the resolution limit in majority ($\approx 99\%$) of sample. In Figure 2, we have shown the one-to-one comparison of $V_c^{out} - V_c^{flat}$. We notice that the V_c^{flat} and V_c^{out} correlates nearly 90% with an intrinsic scatter of 0.03 dex, i.e., for our sample one can either use V_c^{out} or V_c^{flat}. In our analysis, we have used V_c^{out} as a circular velocity and denoted it as V_c.

3.2. Stellar Mass Measurements

We adopt the stellar masses given by Harrison et al. (2017). These stellar masses are computed using fixed mass-to-light ratio in rest-frame H-band, following $M_* = \Upsilon_H \times 10^{-0.4\times(M_H-4.71)}$, where Υ_H and M_H are mass-to-light ratio and absolute magnitude in H-band respectively. Here $\Upsilon_H = 0.2$, which is the median value of our sample derived using the HYPERZ (Bolzonella et al. 2000) Spectral Energy Distribution (SED) fitting tool with a suite of spectral templates from Bruzual & Charlot (2003) using optical to NIR (U, B, V, R, I, J, H, and K) photometry. In some cases, IRAC mid-infrared bands have also been used. For more details, we refer the reader to Harrison et al. (2017). Furthermore, we allow a homogeneous uncertainty of 0.2 dex, which accounts for previous high-z studies (e.g., Stott et al. 2016; Tiley et al. 2019b), typical uncertainty of low and high signal-to-noise photometry, and a possible deviation which may arise by using different tools of SED fitting (for details see Sharma et al. 2021b). The stellar mass range covered by our sample is $8.93 \le \log(M_* \text{ [M}_\odot]) \le 10.97$. A distribution of stellar masses is shown in the right panel of Figure[1].

Note that in Sharma et al. (2021c, under review) we dynamically retrieve the stellar masses of individual and co-added (binned) data. In the same work (Fig.4) we have shown that the dynamically inferred stellar masses of binned data are in one-to-one relation with photometric stellar masses with relatively low intrinsic scatter. Therefore, in this work for individual galaxies we use photometric stellar masses and for binned dataset we use dynamically inferred stellar masses.

3.3. Fitting Method

We consider that the log-log distribution of stellar masses and circular velocities follows a power-law of slope (α) and intercept (β). Which can mathematically defined as:

$$log(Y) = \beta + \alpha \, log(X) \qquad (1)$$

Where, Y can be a list of stellar masses and X circular velocities (V_c). To obtain the best-fit to the data, we use the Generalize Least-square Method (GLM). Which enables to include the uncertainties in the ordinate and abscissa, as well as takes into

---

[3] For an exponential thin disk, stellar-disk radius is defined as $R_D = 0.59R_e$. Under the same assumption, scale length, which encloses the 80% of the stellar mass is referred to the optical radius and defined as $R_{opt} = 3.2R_D$. For details, we refer reader to Persic et al. (1996).

[4] R_{flat} is estimated by taking the median of last three data points in the RCs (assuming RC is flat in the outskirts).
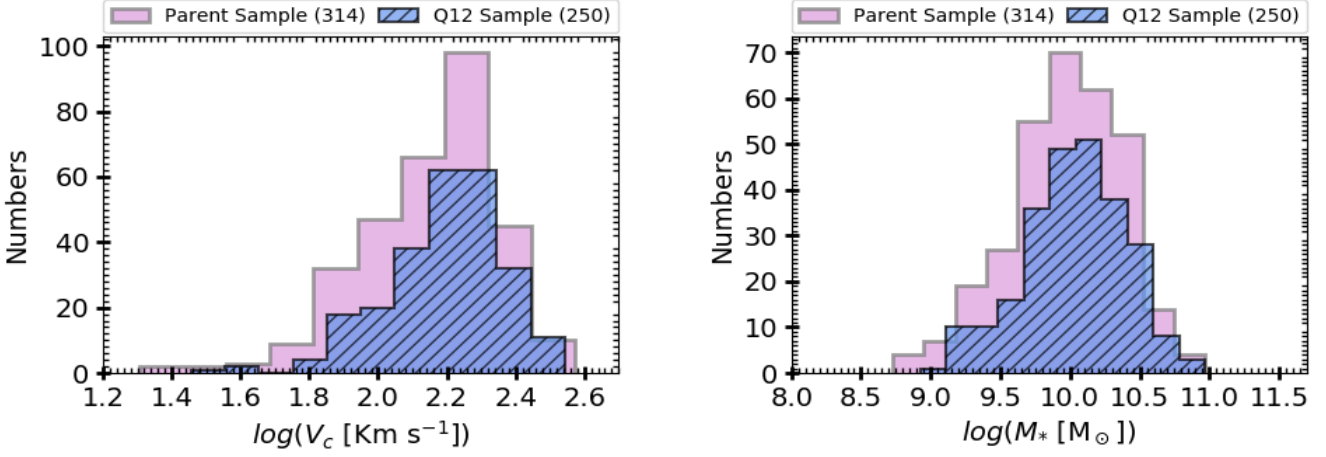
Fig. 1. *Left Panel:* Distribution of circular velocities computed at R_{out} in Sharma et al. (2021a) Sample. *Right panel:* Distribution of stellar masses. The color code in both panels are same and given as following: parent Q12 sample in pink and analysed Q12 sample in blue. Notice Analysed Q12 sample is rotation dominated sample (i.e. $V_{int}/\sigma > 1$) which contain 250 galaxies out of 256, where 6 galaxies are discarded due to huge asymmetry in their rotation curves.
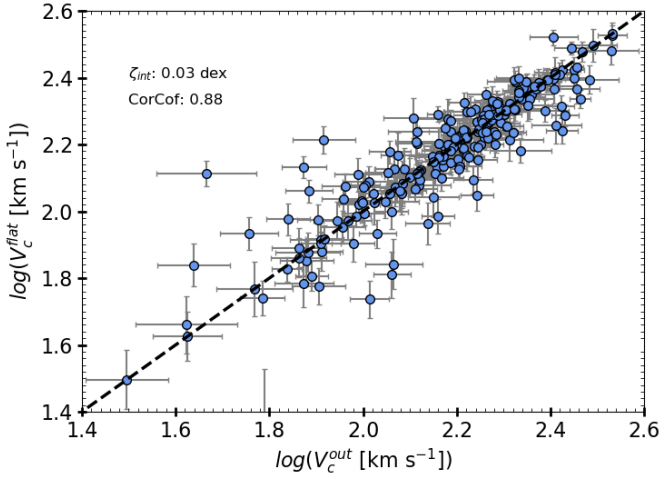

Fig. 2. The comparison of circular velocities computed at R_{out} and R_{flat} (V_c^{out} and V_c^{flat} respectively). The black dashed line is showing the one-to-one plane. The intrinsic scatter (ζ_{int}) and Pearson co-relation coefficient ($CorCof$) are printed on the upper left corner of the plot. In the analysis we refer $V_c^{out} = V_c$ as a circular velocity of object.

account the orthogonal scatter (see Press et al. 1992). For fiducial analysis, we assume maximum likelihood function such that 1) the uncertainties in abscissa and ordinate ($\delta x, \delta y$) are independent of each other, 2) scatter (σ_x, σ_y) in the data is Gaussian. Under this assumption log-likelihood function can be written as:

$$ln(L) = -\sum_{i}^{N} ln\left(\sqrt{2\pi\delta_{y,i}}\right) - \sum_{i}^{N} \frac{(Data - model)^2}{2\delta_{y,i}^2} \qquad (2)$$

where $\delta_{y,i} = \sqrt{\alpha^2\delta_{x,i}^2 + \delta_{y,i}^2 + \sigma_y^2}$, and model is given by equation[1]. This method explores and optimizes the slope and intercept such that it allow minimum intrinsic scatter around the

best-fit. We run the Markov Chain Monte Carlo (MCMC) simulation to obtain the posterior probability distribution of α, β, σ_y. We initialize the chains with 70 random walkers, 10K steps with 5k burn-in. The initial guess are given in the range: $[0 \leq \alpha \leq 5]$, $[1 \leq \beta \leq 10]$, and $[0.01 \leq \sigma_y \leq 2.0]$. This fitting is refer to as 'MCMC-Fit' in the analysis. This kind of method/technique has been previously used to infer the slope of TFR of local galaxies (Lelli et al. 2016), and proven robust to determine the accurate slope and zero-point.

Furthermore, the TFR fitting is performed on normalized data, where normalization is performed around pivot-point (pp) of stellar/baryonic masses and circular velocities. Let us stress that this normalization doesn't not make any change in the slope, but gives an offset on intercept (β_{pp}). This offset is substantially taken-down by computing true intercept (β) as:

$$\beta = -\alpha \times \log(V_c^{pp}) + \log(M^{pp}) - \beta_{pp} \qquad (3)$$

where $\log(V_c^{pp})$ and $\log(M^{pp})$ are the pivot-point of circular velocities ($\log(V_c^{pp}$ [km s^{-1}]) = 2.26) and stellar/baryonic masses ($\log(M_*^{pp}$ [M$_\odot$]) = 10.17, $\log(M_{Bar}^{pp}$ [M$_\odot$]) = 10.35) respectively.

4. Results and Analysis

In this section, we first validate our sample with mass-size and angular momentum scaling relation, and then the new results of Tully-Fisher relation has been shown in comparison with previous high-redshift and local star-forming galaxies.

4.1. Mass-Size Relation

From the theoretical framework of galaxies, we know that the galaxies' halo accrete the hot gas during their evolution process, which cools down at the center of galaxy, as a consequence stars form. Over the time scale of galaxy evolution star-formation takes place in different regions of the galaxy, and from many regions stars eventually migrate. The rotation of galactic halo, which may occur due to tidal torque at the time of formation of halo or during a particular event, also help in migrating the stars
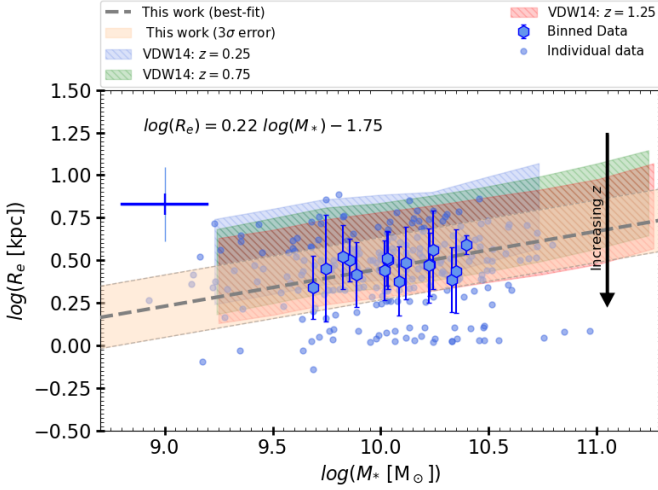
Fig. 3. Mass-size relation of $z \sim 1$ star-forming galaxies compared to van der Wel et al. (2014) (CANDELS survey data). The blue small circles and hexagons represent the data used in this work. The grey dashed line and peach shaded area represent the best fit to the data and the 3σ intrinsic scatter, respectively. The blue, green, and red shaded regions represent the mass-size relation of van der Wel et al. (2014) at $z = 0.25, 0.75,$ and 1.25, respectively. The blue thin and thick plus markers represent the intrinsic scatter of one dex in the individual and binned datasets, respectively, around the grey best-fit line reported in this work.

Binney & Tremaine (2008). Therefore, the study of stellar-mass to size relation gives us the indirect evidence of assembly history of galaxies and their relationship with their dark matter halos.

The two main class of galaxies are early-type and late-type, recognized as red-sequence and blue-cloud in the local Universe (Gavazzi et al. 2010), they both show a different dependency between stellar-disk size and total stellar mass (Shen et al. 2003). However, for nearly a decade, cosmic evolution of mass-size relation of galaxies was an open question, (e.g., early-type: Daddi et al. 2005; van der Wel et al. 2008; Saracco et al. 2011; Carollo et al. 2013; late-type: Mao et al. 1998; Barden et al. 2005; Mosleh et al. 2011). Recently, with a large dataset of CANDELS survey van der Wel et al. (2014) statistically studied the mass-size relation of early- and late-type galaxies through the cosmic time ($0 < z < 3$). They shown that the early type galaxies have steep relation between mass-size, and they evolve faster with time. Whereas, late-type galaxies show a moderate evolution with time, as well as a shallow mass-size relationship, given as:

Early − types :

$$R_e \propto M_*^{0.75} \quad \text{(for } M_* > 2 \times 10^{10} \, \text{M}_\odot\text{)},$$
$$R_e \propto (1 + z)^{-1.48} \quad \text{(fast evolution)} \tag{4}$$

Late − types :

$$R_e \propto M_*^{0.22} \quad \text{(for } M_* > 3 \times 10^9 \, \text{M}_\odot\text{)},$$
$$R_e \propto (1 + z)^{-0.75} \quad \text{(moderate evolution)} \tag{5}$$

It is noteworthy that the intercept of the relation changes while the slope remains the same throughout cosmic time. This suggests that the different assembly mechanism acts similarly on both types of galaxies at different epochs (van der Wel et al.

2014). Thus, we have an empirical evidence for one of the key processes that derive the galaxy evolution.

In this work, we checked our dataset of star-forming disc-like galaxies (i.e. late- types) with the benchmark relation of van der Wel et al. (2014). In Figure 3, we show the mass-size relation of our sample for individual galaxies and binned (derived from co-added RCs) dataset. We applied a liner- fit (using the least-square method) to individual (photometric) and binned (dynamical) quantities. In both cases, we have obtained a similar slope with different intrinsic scatter. In particular, we report a slope of 0.22 which is similar/equal to the one reported in van der Wel et al. (2014), and an intrinsic scatter of 0.21 dex (individuals) and 0.06 dex (binned). This confirms the robustness of photometric and dynamically derived quantities of our sample, and allowed us to investigate the other seminal scaling relations. Furthermore, the authenticity of the mass-size relationship also verifies the robustness of our earlier results in Sharma et al. (2021a,b) and Sharma et al. (2021c, under review).

4.2. Specific Stellar Angular Momentum

The angular momentum is known to be a conserved and fundamental quantity of a galaxy. A galaxy halo acquires angular momentum at the time of its formation through large-scale tidal torques, and it remains approximately constant through-out the subsequent evolution. When the baryons fall into a halo, they can either gain or lose angular momentum (or both) depending on the surrounding conditions. The angular momentum gained by the baryons is generally small when they reach the halo (near the virial radius), but as they approach the centre of the halo (2-10 kpc), they can gain enough angular- momentum to form a centrifugally supported disc that follows an exponential profile (Athanassoula 1983; Mo et al. 1998). From observations of local galaxies we know that in the latter processes the angular momentum seems to decay (re-distributed) weakly, i.e. a fraction ($\sim$ 30%) of it is lost (transferred), either by viscus angular momentum redistribution (e.g. Courteau 1997), or due to gas losses during disc formation (e.g. Burkert 2009). Numerical framework of galaxy evolution suggest that angular momentum transfer occurs when the galactic disc is sufficiently centrifugally supported, roughly around $z \sim 1$ (Lagos et al. 2017). However, it is currently a major challenge to provide observational evidence in favour of the latter. Recently, some IFU studies (e.g. Obreschkow et al. 2015; Burkert et al. 2016; Swinbank et al. 2017; Gillman et al. 2020) have shown that the stellar angular momentum scaling relation with stellar mass follow $J_* = M_*^{2/3}(1+z)^{-\alpha}$ relation, where $(1+z)^{-\alpha}$ with $\alpha = 0.51.5$, gives the cosmic evolution, i.e. angular momentum transfer over cosmic time, which is very minimal for star-forming galaxies.

Given the moderate resolution in our sample (similar to previous high-redshift studies) but differently processed kinematics (relative to previous high-redshift studies). In this work, we attempted to verify the stellar angular momentum scaling with stellar (and halo) mass, relative to previously mentioned studies. Following Romanowsky & Fall (2012) we compute the stellar angular momentum normalized to stellar mass, i.e. specific stellar angular momentum, because it removes the implicit scaling between angular momentum and stellar mass:

$$j_*^n = k_n V_c R_e \tag{6}$$

where, V_c is the circular velocity of the galaxy, R_e is the effective radius, and k_n depends on the sérsic index of galaxy which can be approximated by $k_n = 1.15 + 0.029n + 0.062n^2$.
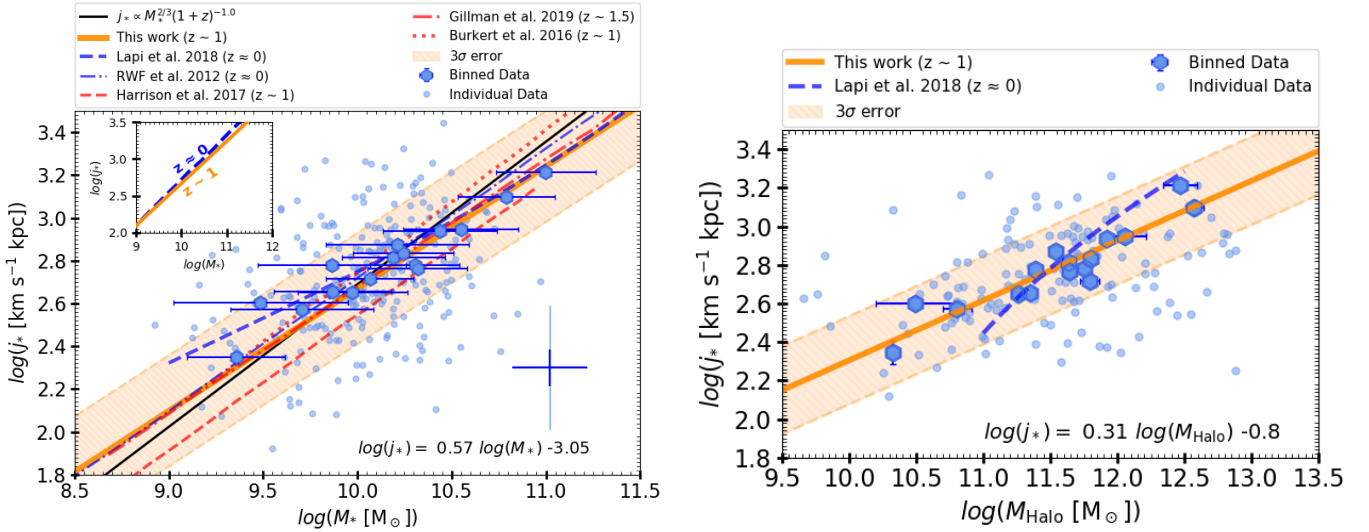
Fig. 4. Specific stellar angular momentum as a function of stellar and halo mass, left and right panels, respectively. The blue circles and hexagons represent the individual and binned dataset. The orange solid line and peach shaded area represent the best fit to the data and the intrinsic scatter of 3σ, respectively. The comparison studies of local star-forming galaxies are indicated by blue dotted-dashed and dashed lines, Romanowsky & Fall (2012) and Lapi et al. (2018), respectively; high-redshift studies are represented by the red dotted, dotted-dashed, and dashed lines, Burkert et al. (2016); Harrison et al. (2017), and Gillman et al. (2020), respectively. The black solid line shows the relation $J_* = M_*^{2/3}(1 + z)^{\alpha}$ with $\alpha = 1.0$ (Swinbank et al. 2017), which is very close to the data, and shows an intrinsic scatter of 0.06dex (for binned data). This shows that we are in good agreement with previous studies (Burkert et al. 2016; Swinbank et al. 2017). The blue thin and thick plus markers represent the intrinsic scatter of one dex in the individual and binned datasets, respectively, around the orange best-fit line. The inset-figure in the left panel shows a zoom of $j_* - M_*$ fits at $z \sim 1$ (this work) and $z \approx 0$ (Romanowsky & Fall 2012) within the stellar mass range $9.0 \leq log(M_* \, [M_\odot]) \leq 12.0$.

To calculate the j_* of our sample, we use the circular velocity computed at 2.95 R_e, and the sérsic index of our sample ranges between $0.65 \leq n \leq 1.25$; therefore, we approximated n=0.95 ± 0.2. To fit the slope to the relation we use the same procedure defined for SFTR in Section 3.3. The results are shown in the left panel of Figure 4. We note that the best- fit obtained in our work is equivalent to the fit obtained by Swinbank et al. (2017) and Gillman et al. (2020). Moreover, we matches the previous local and other high-redshift studies within 3σ uncertainty.

A consistency check of the $j_* - M_*$ best-fits for a typical range of stellar masses ($9.0 \leq log(M_* \, [M_\odot]) \leq 12.0$) of local disc galaxies is shown in the inset of the left panel of Figure 4, for $z \sim 1$ and $z \approx 0$ galaxies. As we can see, $j_* - M_*$ shows a very minimal (or no) change in the slope and zero-point of the relation. The similarity of the $j_* - M_*$ plain of this work and other studies justifies the robustness of the kinematic and dynamical methods used in our previous works (Sharma et al. 2021a,b,c). Therefore, now we can confidently use our sample to investigate the STFR over cosmic time-scales. On the other hand, the scaling of the specific angular momentum with the halo mass, right panel Figure 4, shows a divergent evolution over cosmic time. This suggests that most-likely interplay (gravitational or collisional) between dark and luminous matter strongly depends on the environment, which we will investigate in our future work.

4.3. Stellar Tully-Fisher Relation

Using the method described in Section 3.3, we obtained the best fit to the $M_* - V_c$ plain of $z \sim 1$ star-forming galaxies, the so-called 'Stellar Tully-Fisher Relation (STFR),' which is shown in Figure 5. We fitted both the individual galaxies (orange circles), and the binned dataset (orange hexagons). However, we have shown the best-fit corresponds to the binned dataset, as we

rely on dynamically derived stellar masses more than the photometric stellar masses (see Sharma et al. 2021c). We find that all individual data points fall within the 3σ scatter of the best-fit (taking into account the 0.2 dex uncertainty of the individual stellar masses, see Section 3.2). We report STFR slope of $\alpha_s = 2.43 \pm 0.85$ and zero-point $\beta_s/\alpha_s = 2.00 \pm 0.44$, with an intrinsic scatter of 0.4 dex (individuals) and 0.21 dex (binned).

To compare our results with local star-forming galaxies, we adopt the slope and intercept of the STFR relation given by Reyes et al. 2011 and Lapi et al. 2018. One can note that our results are comparable to both local studies within 3σ uncertainty. However, the intrinsic scatter reported around the best-fit of the comparison studies is a factor of 2 higher than the best-fit obtained in our work. Moreover, in this work we intend to investigate the small deviation between the slope and the zero-point of the STFR at two epochs ($z \approx 0$ and $z \sim 1$). Therefore, we decided to closely compare the slope and zero-point obtained in this work with those obtained for the local population (in particular Lapi et al. 2018) within the range of circular velocity $log(Vc \, [km \, s^{-1}]) = 1.8 - 3.0$, and stellar mass $log(M_* \, [M_\odot]) = 9.0 - 12.0$, shown in the inset of Figure 5.[5] We have found that the STFR shows a divergent evolution between $z \sim 1$ and $z \approx 0$ in the given mass and velocity range. That is, the zero-point of the relation does not change with cosmic time, while the slope shows a significant evolution.

To compare the results with those of high-redshift star-forming galaxies, we used the relations reported by Di Teodoro et al. (2016); Tiley et al. (2019a) and Übler et al. (2017), details are given in Table .1. We note that all of the aforementioned studies fairly accurately reflect our data. However, to assess the

---

[5] $1.8 \leq log(Vc \, [km \, s^{-1}]) \leq 3.0$ and $9.0 \leq log(M_* \, [M_\odot]) \leq 12.0$ are typical circular velocity and stellar mass ranges of local star-forming galaxies, respectively.
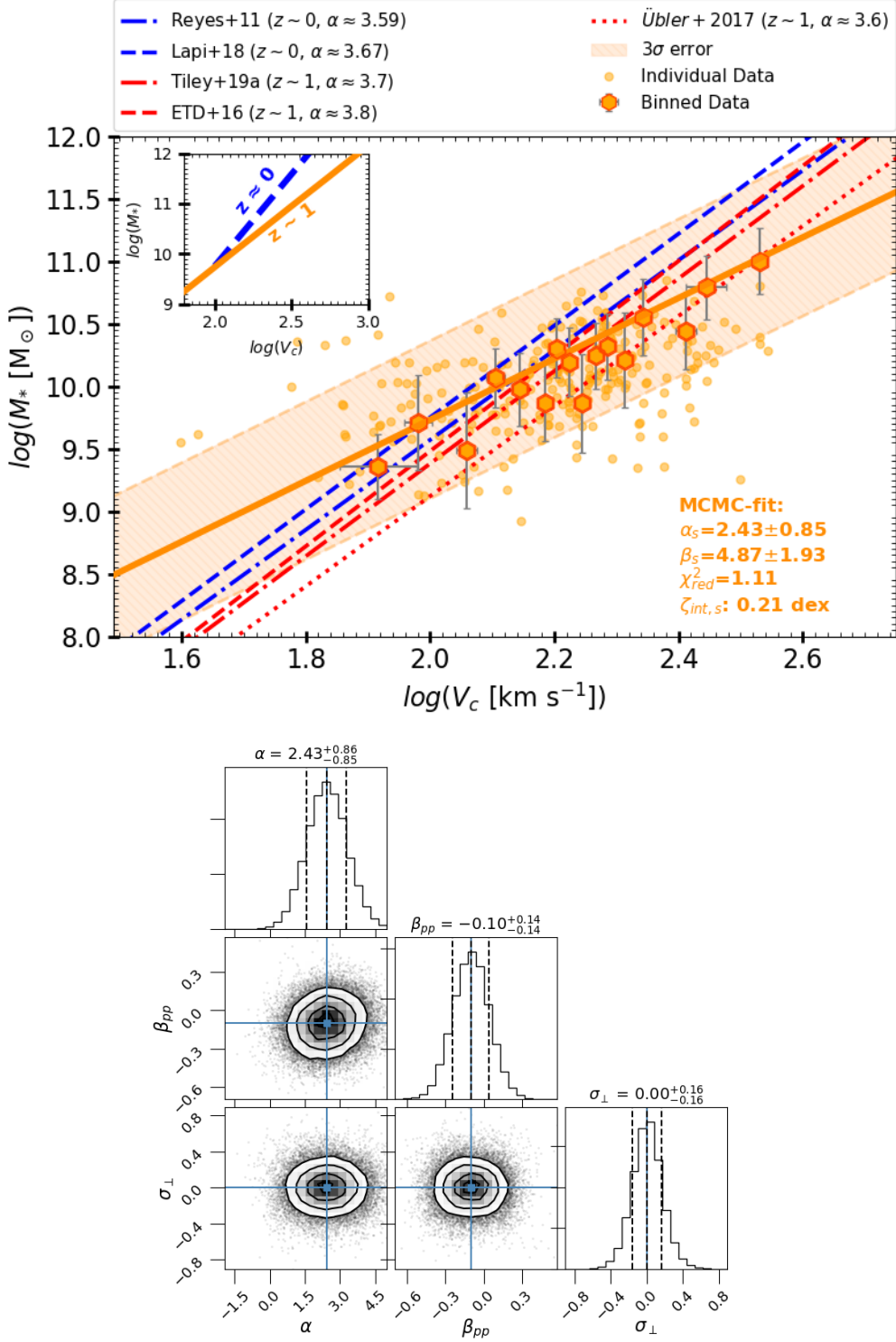
Fig. 5. *Upper panel:* Stellar Tully-Fisher relation of $z \sim 1$ star-forming galaxies. The orange circle, and hexagons represents the individual and binned data. The solid orange line shows the best-fit to the data generated using MCMC sampling, the dashed orange lines followed by the shaded area represents the 3σ intrinsic scatter around the best fit line. The quality assessment parameters (χ^2_{red}, $\zeta_{int,s}$) of MCMC-fit are printed on the lower-right side of the plot. For comparison purpose, we have plotted the local and high-z STFRs by blue and red lines, respectively. Local STFR: The blue dotted-dashed line represents the Reyes et al. (2011) relation, and the blue dashed line shows the Lapi et al. (2018) relation. High-z STFR: the red dashed, dotted, and dotted-dashed lines show the Di Teodoro et al. (2016); Übler et al. (2017), and Tiley et al. (2019a), respectively. The inset-figure shows the zoom of STFR-fits at $z \sim 1$ (this work) and $z \approx 0$ (Lapi et al. 2018) within the range of circular velocity $log(Vc$ [km s^{-1}]$) = 1.8 - 3.0$, and stellar mass $log(M_*$ [M$_\odot$]$) = 9.0 - 12.0$. *Lower panel:* Posterior distribution of MCMC-fit, α is the slope, β_{pp} is intercept (offset around pivot-point: pp), and $\sigma_\perp$ is the scatter on y-axis data. The blue crosses in the corner plots shows the final best-fit values, and they are printed on the top of each posterior distribution. Notice, in the main text (and plots) notation for slope, intercept and intrinsic scatter are referred to as α_s, β_s, and $\zeta_{int,s}$ for STFR.

correctness of their best fit with respect to our data, we calculate the intrinsic scatter around their fits. We found that the intrinsic scatter with respect to other fits is at least a factor of 1 higher than the one obtained in our work, see Table .1. Therefore, we rely on the best fit, which we have obtained using a state-of-the-art technique. Moreover, small discrepancies in the slope and zero-point may result from differences in the determination of the circular velocities (kinematics), mentioned in Section 1.

5. Discussion and Conclusions

Recent studies of high-redshift galaxies, in particular Tiley et al. (2019a, KROSS) and Übler et al. (2017, KMOS3D), largely referred and compared with our earlier works, report that the zero-point of the STFR varies with cosmic time, while the slope remains the same. In contrast to both studies, we report a significant evolution of the slope while the zero-point remains constant in the range of circular velocity $log(Vc \text{ [km s}^{-1}\text{]}) = 1.8 - 3.0$, and stellar mass $log(M_* \text{ [M}_\odot\text{]}) = 9.0 - 12.0$, which is a similar range studied by Tiley et al. (2019a) and Übler et al. (2017). In particular, we report a divergent evolution in STFR from $z \sim 1$ to $z \approx 0$, as shown in Figure 5.

First of all, the evolution in the STFR and no evolution in mass-size and $J_* - M_*$ relation of star-forming galaxies suggests that the baryonic assembly works in a similar way at all epochs in these systems. While, the dark matter response to the baryonic process is most likely different and time-dependent. Secondly, divergent evolution in the STFR (and also in $J_* - M_{\text{Halo}}$ relation) may occur in response to environmental changes, for example, accretion and ejection of mass. Alternatively, divergent evolution may also takes place in response to the change/stabilisation of pressure conditions at high-redshift.

On the other hand, comparing our previous findings of Sharma et al. (2021a) and Sharma et al. (2021b) with current work, we found that:

at $z \sim 1$:

$$M_* \propto V_c^{2.43} \rightarrow V_c \propto M_*^{0.41} \quad \& \quad V_c \propto R_D^0 \tag{7}$$

that is, circular velocity does not depend on stellar-disk radius, and quickly grows with stellar mass. Whereas for locals:

at $z \approx 0$:

$$M_* \propto V_c^4 \rightarrow V_c \propto M_*^{0.25} \quad \& \quad V_c \propto R_D^{0.67} \tag{8}$$

that is, circular velocity has nearly linear relation with stellar-disk radius of galaxies (Lapi et al. 2018) and grows slowly with stellar mass. Alternatively, Equations 7 & 8 are suggesting that the for given a stellar mass gravitational potential ($V_c^2 = rd\Phi/dr$) experienced by a galaxy at $z \sim 1$ is higher than at $z \approx 0$, independent of its radius. This means that the galaxy with a same stellar masses have higher dark matter content within stellar disc. The latter results have already been reported using a model independent dynamical studies of rotation curves (Sharma et al. 2021b), where we show that dark matter fraction $f_{\text{DM}}(< R_{opt} \text{ at } z \approx 0)$ is smaller than $f_{\text{DM}}(< R_{opt} \text{ at } z \sim 1)$.

Furthermore, if star-formation is always inside-out in disc-like systems (Moster et al. 2018), i.e. baryon ensembles and turns into stars in similar manner at $z \sim 1$ and $z \approx 0$. On the other hand, Sharma et al. (2021b) we have already shown that the contribution of gas to the circular velocity is minimal, i.e. $V_c^2 \approx V_{\text{star}}^2 + V_{\text{DM}}^2$. Then, the evolution in the slope of STFR also suggest an evolution in the dark matter distribution. Surprisingly, the latter finding have also been reported by us in our

recent paper Sharma et al. (2021c, in peer review) using dynamical mass-modelling of rotation curves. These results can easily be favoured by phenomena, such as feedback scenarios and dynamical heating due to bursty star-formation which may transform dark matter *cusp* into *core* over the cosmic time (Navarro et al. 1996; Pontzen & Governato 2012; Nipoti & Binney 2014; Read et al. 2016; Lazar et al. 2020). Moreover, we would like to point-out that the large scatter in the relation (in individual data-points) is possibly indicating the kinematic and morphological transition of high-z galaxies, which has also been reported by Kassin et al. (2007); Miller et al. (2014); Simons et al. (2016) and Übler et al. (2017).

6. Summary

In this paper, we studied the seminal scaling relation, the 'Tully-Fisher relation' of star-forming galaxies since $z \sim 1$. We exploit the kinematic and photometric data obtained in Sharma et al. (2021a) and Sharma et al. (2021b). In particular we use 250 high-quality rotation dominated galaxies from the Q12 sample studied in Sharma et al. (2021a). This sample lies between redshift $0.7 \lesssim z \lesssim 1.0$ with stellar masses $log(M_* \text{ [M}_\odot\text{]}) = 9.0 - 11.0$ and circular velocities $log(V_{out} \text{ km s}^{-1}) = 1.45 - 2.53$. The rotation curves of the Q12 sample (individual and co-added) are dynamically modelled to decompose them into their constituents (stars, gas, and dark matter) to study the structural properties of dark matter, see Sharma et al. (2021c, under peer review). The latter work also provides dynamically derived stellar and halo masses, which we have also employed in this work, especially in case of binned data.

In our earlier work, we have already demonstrated the robustness of circular velocities, which we compute using slightly different techniques than those employed in the recent high-redshift literature. In this work, we first showed the correctness of our photometric quantities: stellar mass and size, by plotting the mass-size relation of star-forming galaxies. We have demonstrated that our sample correctly reproduces the mass-size relation of $z \sim 1$ star-forming galaxies given by van der Wel et al. (2014), see Section 4.1. We have also shown that the scaling relation of stellar angular momentum with stellar mass emerges very similar to the previous studies of high-redshift star-forming galaxies (Burkert et al. 2016; Swinbank et al. 2017), see Figure 4. Verification of both, mass-size and $j_* - M_*$ relations, assure our kinematics and dynamical measurements. Therefore, we then exploited the stellar mass and circular velocity information to demonstrate the Stellar Tully-Fisher Relation (STFR), see Section 4.3. The fitting is performed using a state-of-the-art method (Section 3.3), that has been proven to be robust for fitting the Tully-Fisher relation of local star-forming galaxies (e.g. Lelli et al. 2016). Furthermore, our results are compared with local and high-redshift STFR studies, see Section 4.3 & 5. We find that all previous studies fit the data fairly closely within the uncertainty of 3σ. A large scatter in the relation (for individual data) is possibly indicative of the kinematic and morphological transition of high-redshift galaxies.

Although previous studies are largely consistent with our results, in this work, we intend to accurately measure the difference in slope and zero- point of STFR between $z \approx 0$ and $z \sim 1$. Therefore, we compared the STFR fit obtained in our work with that of Lapi et al. 2018 (representing the local counterparts of $z \sim 1$ star-forming galaxies). The results are shown in the inset of the Figure 5. We find that between $1.8 \leq log(Vc \text{ [km s}^{-1}\text{]}) \leq 3.0$ and $9.0 \leq log(M_* \text{ [M}_\odot\text{]}) \leq 12.0$ the zero- point remains the same, while the slope of the relation evolves. In particular, **we re-**

port a *divergent evolution* in the STFR through cosmic time.
The latter suggests that the interplay of dark and luminous matter
within the galaxies is strongly environment dependent process,
i.e., galactic process do affect the distribution of dark matter in
their subsequent evolution .

References

Athanassoula, E. E., ed. 1983, Internal kinematics and dynamics of galaxies, ed. E. E. Athanassoula, Vol. 100

Barden, M., Rix, H.-W., Somerville, R. S., et al. 2005, ApJ, 635, 959

Bell, E. F. & de Jong, R. S. 2001, The Astrophysical Journal, 550, 212

Binney, J. & Tremaine, S. 2008, Galactic Dynamics: Second Edition (Princeton University Press)

Blumenthal, G. R., Faber, S., Primack, J. R., & Rees, M. J. 1984, Nature, 311, 517

Böhm, A., Ziegler, B. L., Saglia, R. P., et al. 2004, A&A, 420, 97

Bolzonella, M., Miralles, J. M., & Pelló, R. 2000, A&A, 363, 476

Bruzual, G. & Charlot, S. 2003, MNRAS, 344, 1000

Burkert, A. 2009, in Astronomical Society of the Pacific Conference Series, Vol. 419, Galaxy Evolution: Emerging Insights and Future Challenges, ed. S. Jogee, I. Marinova, L. Hao, & G. A. Blanc, 3

Burkert, A., Genzel, R., Bouché, N., et al. 2010, The Astrophysical Journal, 725, 2324

Burkert, A., Schreiber, N. F., Genzel, R., et al. 2016, The Astrophysical Journal, 826, 214

Carollo, C. M., Bschorr, T. J., Renzini, A., et al. 2013, ApJ, 773, 112

Conselice, C. J., Blackburne, J. A., & Papovich, C. 2005, The Astrophysical Journal, 620, 564

Courteau, S. 1997, AJ, 114, 2402

Cresci, G., Hicks, E. K. S., Genzel, R., et al. 2009, The Astrophysical Journal, 697, 115

Daddi, E., Renzini, A., Pirzkal, N., et al. 2005, ApJ, 626, 680

de Blok, W. J. G., Walter, F., Brinks, E., et al. 2008, AJ, 136, 2648

Di Teodoro, E., Fraternali, F., & Miller, S. 2016, Astronomy & Astrophysics, 594, A77

Feast, M. W. 1994, MNRAS, 266, 255

Ferrarese, L., Ford, H. C., Huchra, J., et al. 2000, ApJS, 128, 431

Foreman, S. & Scott, D. 2012, Phys. Rev. Lett., 108, 141302

Freedman, W. L., Madore, B. F., Scowcroft, V., et al. 2011, AJ, 142, 192

Gavazzi, G., Fumagalli, M., Cucciati, O., & Boselli, A. 2010, A&A, 517, A73

Gillman, S., Tiley, A. L., Swinbank, A. M., et al. 2020, MNRAS, 492, 1492

Giovanelli, R., Haynes, M. P., da Costa, L. N., et al. 1997a, ApJ, 477, L1

Giovanelli, R., Haynes, M. P., Herter, T., et al. 1997b, AJ, 113, 53

Girardi, M., Manzato, P., Mezzetti, M., Giuricin, G., & Limboz, F. 2002, The Astrophysical Journal, 569, 720

Gnerucci, A., Marconi, A., Cresci, G., et al. 2011, A&A, 528, A88

Harrison, C., Johnson, H., Swinbank, A., et al. 2017, Monthly Notices of the Royal Astronomical Society, 467, 1965

Johnson, H. L., Harrison, C. M., Swinbank, A. M., et al. 2018, Monthly Notices of the Royal Astronomical Society, 474, 5076

Karachentsev, I. D., Mitronova, S. N., Karachentseva, V. E., Kudrya, Y. N., & Jarrett, T. H. 2002, A&A, 396, 431

Kassin, S. A., Weiner, B. J., Faber, S. M., et al. 2007, ApJ, 660, L35

Lagos, C. D. P., Baugh, C. M., Lacey, C. G., et al. 2011, MNRAS, 418, 1649

Lagos, C. d. P., Theuns, T., Stevens, A. R. H., et al. 2017, MNRAS, 464, 3850

Lapi, A., Salucci, P., & Danese, L. 2018, The Astrophysical Journal, 859, 2

Lazar, A., Bullock, J. S., Boylan-Kolchin, M., et al. 2020, arXiv e-prints, arXiv:2004.10817

Lelli, F., McGaugh, S. S., & Schombert, J. M. 2016, ApJ, 816, L14

Lelli, F., McGaugh, S. S., Schombert, J. M., Desmond, H., & Katz, H. 2019, Monthly Notices of the Royal Astronomical Society, 484, 3267

Madau, P. & Dickinson, M. 2014, Annual Review of Astronomy and Astrophysics, 52, 415

Mao, S., Mo, H. J., & White, S. D. M. 1998, Monthly Notices of the Royal Astronomical Society, 297, L71

Masters, K. L., Springob, C. M., Haynes, M. P., & Giovanelli, R. 2006, The Astrophysical Journal, 653, 861

Mathewson, D. S., Ford, V. L., & Buchhorn, M. 1992, ApJS, 81, 413

McGaugh, S. S. 2005, Phys. Rev. Lett., 95, 171302

McGaugh, S. S., Schombert, J. M., Bothun, G. D., & de Blok, W. J. G. 2000, The Astrophysical Journal, 533, L99

Miller, S. H., Bundy, K., Sullivan, M., Ellis, R. S., & Treu, T. 2011, ApJ, 741, 115

Miller, S. H., Ellis, R. S., Newman, A. B., & Benson, A. 2014, The Astrophysical Journal, 782, 115

Miller, S. H., Ellis, R. S., Sullivan, M., et al. 2012, The Astrophysical Journal, 753, 74

Mo, H. J. & Mao, S. 2000, Monthly Notices of the Royal Astronomical Society, 318, 163

Mo, H. J., Mao, S., & White, S. D. M. 1998, MNRAS, 295, 319

Mosleh, M., Williams, R. J., Franx, M., & Kriek, M. 2011, ApJ, 727, 5

Moster, B. P., Naab, T., & White, S. D. M. 2018, Monthly Notices of the Royal Astronomical Society, 477, 1822

Navarro, J. F., Eke, V. R., & Frenk, C. S. 1996, Monthly Notices of the Royal Astronomical Society, 283, L72

Neill, J. D., Seibert, M., Tully, R. B., et al. 2014, ApJ, 792, 129

Nipoti, C. & Binney, J. 2014, Monthly Notices of the Royal Astronomical Society, 446, 1820

Obreschkow, D., Glazebrook, K., Bassett, R., et al. 2015, The Astrophysical Journal, 815, 97

Papastergis, E., Adams, E. A. K., & van der Hulst, J. M. 2016, A&A, 593, A39

Pérez-González, P. G., Rieke, G. H., Villar, V., et al. 2008, The Astrophysical Journal, 675, 234

Persic, M., Salucci, P., & Stel, F. 1996, Monthly Notices of the Royal Astronomical Society, 281, 27

Pizagno, J., Prada, F., Weinberg, D. H., et al. 2007, AJ, 134, 945

Pontzen, A. & Governato, F. 2012, Monthly Notices of the Royal Astronomical Society, 421, 3464

Press, W. H., Teukolsky, S. A., Vetterling, W. T., & Flannery, B. P. 1992, Numerical recipes in FORTRAN. The art of scientific computing (Cambridge University Press)

Puech, M., Flores, H., Hammer, F., et al. 2008, A&A, 484, 173

Read, J., Iorio, G., Agertz, O., & Fraternali, F. 2016, Monthly Notices of the Royal Astronomical Society, 462, 3628

Reyes, R., Mandelbaum, R., Gunn, J., Pizagno, J., & Lackner, C. 2011, Monthly Notices of the Royal Astronomical Society, 417, 2347

Romanowsky, A. J. & Fall, S. M. 2012, ApJS, 203, 17

Saracco, P., Longhetti, M., & Gargiulo, A. 2011, Monthly Notices of the Royal Astronomical Society, 412, 2707

Sharma, G., Salucci, P., Harrison, C. M., van de Ven, G., & Lapi, A. 2021a, Monthly Notices of the Royal Astronomical Society, 503, 1753

Sharma, G., Salucci, P., & van de Ven, G. 2021b, Astronomy & Astrophysics, 503, 1753

Sharma, G., Salucci, P., & van de Ven, G. 2021c, A&A, 000, 0000

Shen, S., Mo, H. J., White, S. D. M., et al. 2003, MNRAS, 343, 978

Simons, R. C., Kassin, S. A., Trump, J. R., et al. 2016, The Astrophysical Journal, 830, 14

Sorce, J. G., Courtois, H. M., Tully, R. B., et al. 2013, ApJ, 765, 94

Stark, D. V., McGaugh, S. S., & Swaters, R. A. 2009, AJ, 138, 392

Steinmetz, M. & Navarro, J. F. 1999, ApJ, 513, 555

Stott, J. P., Swinbank, A., Johnson, H. L., et al. 2016, Monthly Notices of the Royal Astronomical Society, 457, 1888

Swinbank, A. M., Harrison, C. M., Trayford, J., et al. 2017, Monthly Notices of the Royal Astronomical Society, 467, 3140

Tacconi, L. J., Genzel, R., Saintonge, A., et al. 2018, ApJ, 853, 179

Teodoro, E. D. & Fraternali, F. 2015, Monthly Notices of the Royal Astronomical Society, 451, 3021

Tiley, A., Bureau, M., Cortese, L., et al. 2019a, Monthly Notices of the Royal Astronomical Society, 482, 2166

Tiley, A. L., Stott, J. P., Swinbank, A. M., et al. 2016, MNRAS, 460, 103

Tiley, A. L., Swinbank, A., Harrison, C., et al. 2019b, Monthly Notices of the Royal Astronomical Society, 485, 934

Toribio, M. C., Solanes, J. M., Giovanelli, R., Haynes, M. P., & Martin, A. M. 2011, ApJ, 732, 93

Tully, R. B. & Fisher, J. R. 1977, Astronomy and Astrophysics, 54, 661

Tully, R. B. & Pierce, M. J. 2000, ApJ, 533, 744

Turner, O. J., Harrison, C. M., Cirasuolo, M., et al. 2017, arXiv e-prints, arXiv:1711.03604

Übler, H., Förster Schreiber, N. M., Genzel, R., et al. 2017, ApJ, 842, 121

Valenzuela, O., Rhee, G., Klypin, A., et al. 2007, The Astrophysical Journal, 657, 773

van der Wel, A., Franx, M., van Dokkum, P. G., et al. 2014, ApJ, 788, 28

van der Wel, A., Holden, B. P., Zirm, A. W., et al. 2008, ApJ, 688, 48

van Starkenburg, L., van der Werf, P. P., Yan, L., & Moorwood, A. F. M. 2006, arXiv e-prints, astro

Verheijen, M. A. W. & Sancisi, R. 2001, A&A, 370, 765

Weijmans, A.-M., Krajnović, D., Van De Ven, G., et al. 2008, Monthly Notices of the Royal Astronomical Society, 383, 1343

Wellons, S., Faucher-Giguère, C.-A., Anglés-Alcázar, D., et al. 2020, Monthly Notices of the Royal Astronomical Society, 497, 4051

Ziegler, B. L., Böhm, A., Fricke, K. J., et al. 2002, The Astrophysical Journal, 564, L69

Author	Relation	Redshift	α_s [log($km\ s^{-1}$)]	β_s [log($M_\odot$)]	χ^2_{red}	$\zeta_{int,s}$ (dex)
This work	STFR	$z \sim 1$	2.43 ± 0.85	2.00 ± 0.44	1.11	0.21
Reyes et al. (2011)	STFR	$z \sim 0$	$\approx 3.59 \pm 0.01$	$\approx 2.39 \pm 0.01$	2.34	0.34
Lapi et al. (2018)	STFR	$z \sim 0$	$\approx 3.67 \pm 0.23$	$\approx 2.41 \pm 0.10$	2.79	0.51
Di Teodoro et al. (2016)	STFR	$z \sim 1$	$\approx 3.80 \pm 0.21$	$\approx 1.88 \pm 0.46$	2.34	0.33
Übler et al. (2017)	STFR	$z \sim 1$	$\approx 3.60 \pm 0.01$	$\approx 1.92 \pm 0.01$	2.38	0.32
Tiley et al. (2019a)	STFR	$z \sim 1$	$\approx 3.70 \pm 0.3$	$\approx 9.88 \pm 0.10$	2.22	0.27

Table .1. Stellar Tully Fisher Relation slope and zero-points obtained in this work and previous studies. Here $\alpha_s, \beta_s, \chi^2_{red}$, and $\zeta_{int,s}$ columns gives the slope, zero-point, reduced χ-square relative to data used in this work, and intrinsic scatter around the best-fit, respectively.